We are IntechOpen,
the world's leading publisher of
Open Access books
Built by scientists, for scientists

6,900
Open access books available

186,000
International authors and editors

200M
Downloads

Our authors are among the

154
Countries delivered to

TOP 1%
most cited scientists

12.2%
Contributors from top 500 universities

BOOK CITATION INDEX
CLARIVATE ANALYTICS
INDEXED

WEB OF SCIENCE™

Selection of our books indexed in the Book Citation Index
in Web of Science™ Core Collection (BKCI)

Interested in publishing with us?
Contact book.department@intechopen.com

Propagating Surface Plasmons and Dispersion Relations for Nanoscale Multilayer Metallic-Dielectric Films

Henrique T. M. C. M. Baltar, Krystyna Drozdowicz-Tomsia and Ewa M. Goldys

Additional information is available at the end of the chapter

1. Introduction

The study of propagating surface plasmons (PSPs) is an important aspect of the understanding of the interaction between light and metallic surfaces. One of the key concepts related to PSPs, is the dispersion relation. This relation is the basis for understanding of coupling of light to PSPs, by using special approaches to match the wavevector. Moreover, it can be used to predict the matching of localised surface plasmons (LSPs) and PSPs to achieve highly enhanced electromagnetic field and/or tailored transmission.

This chapter is concerned with a detailed analysis of propagating surface plasmons (PSPs), and the calculations of the dispersion relations in nanoscale multilayer metallic-dielectric films, starting from the fundamental Maxwell's equations. Furthermore, we discuss the symmetric IMI (insulator-metal-insulator) and MIM (metal-insulator-metal) geometries, as well as their asymmetric variants. We will also describe the PSP in the IIMI (insulator-insulator-metal-insulator) geometry.

There is a vast literature on the subject, however, numerous authors assume the materials as lossless by using the Drude's model without damping. We initially model the dielectric function of the metals in our multilayer structures by using the lossless Drude's model. Then, we model the metals by applying complex values of permittivities acquired experimentally. The Drude's model without damping, with its simplicity, provides a basic understanding, as all the calculated quantities are purely real or imaginary numbers. Nevertheless, real structures behave differently from the predictions of this simple model. The dispersion relation changes markedly, when complex permittivities are used, and the changes are more pronounced around the surface plasmon frequency. This leads to wavevector limitations and to the existence of a region of anomalous dispersion, called quasi-bound mode [4]. Therefore, it is necessary to extend the analysis to include complex permittivity, which has been tabulated for the most common materials.

There are some previous studies on the behaviour of the IMI and MIM structures using complex permittivity, but the discussions are restrained to symmetric structures and/or do not show the entire dispersion curve [4, 5, 32]. In many cases, such symmetries are not applicable to the real experiments. For instance, assays with analytes deposited over a metallic layer on a substrate are, in this sense, an asymmetric problem.

Other experimentally important structure is the IIMI. Such structure is used for surface-enhanced fluorescence (SEF). A dielectric separation layer between metal and fluorophore can be introduced to maximise the fluorescence by reducing the possibility of quenching of fluorophores in direct contact with metal surfaces [6]. To the best of our knowledge, there are no published studies of the dispersion relation for such type of asymmetric structures. These new calculations are presented in this work.

2. Permittivity of metals

The Drude's model, taking into account only free electrons, is applicable to metals and leads to the following expression for the relative permittivity [16, 23]:

$$\varepsilon_r = 1 - \frac{\omega_p^2}{\omega^2 + i\Gamma\omega} \tag{1}$$

Here, ω_p is called the plasma frequency, and the damping constant Γ is the electron scattering rate (the inverse of the collision time for the conduction electrons). When a metal is assumed lossless (very long time between collisions, $\Gamma \to 0$), the permittivity becomes real:

$$\text{Drude's permittivity without damping:} \quad \varepsilon_r = 1 - \frac{\omega_p^2}{\omega^2} \tag{2}$$

In this study, we also model the metal permittivity by the tabulated values of silver from Lynch and Hunter [20]. In the case of asymmetric MIM geometry, we will also use the tabulated permittivity of gold from Johnson and Christy [13]. In Figure 1, we plotted the real and imaginary parts of the permittivities of silver and gold. For the Drude's model without damping, we used the plasma frequency of 13.1 Prad (2.08 PHz, $\lambda_p = 144$ nm) for silver and 13.4 Prad (2.13 PHz, $\lambda_p = 141$ nm) for gold.

3. Theoretical framework

3.1. Source-free Maxwell's equations in time-harmonic regime

The Maxwell's equations hold for any arbitrary time-dependence of the electric field. For materials in a linear regime we can consider these equations for each frequency component separately [1]. The time-dependent electric or magnetic fields can be written as the real part of a complex field, denoted by F:

$$\vec{F}(\vec{r}, t) = \vec{F}_0(\vec{r}) \cos\left(\vec{k} \cdot \vec{r} - \omega t + phase\right) = Re\left[\vec{F}(\vec{r}) e^{-i\omega t}\right] \tag{3}$$

---

[1] The non-linear regime is when the material properties such as permittivity and permeability depend on frequency and intensity of the field, and will not be considered here.
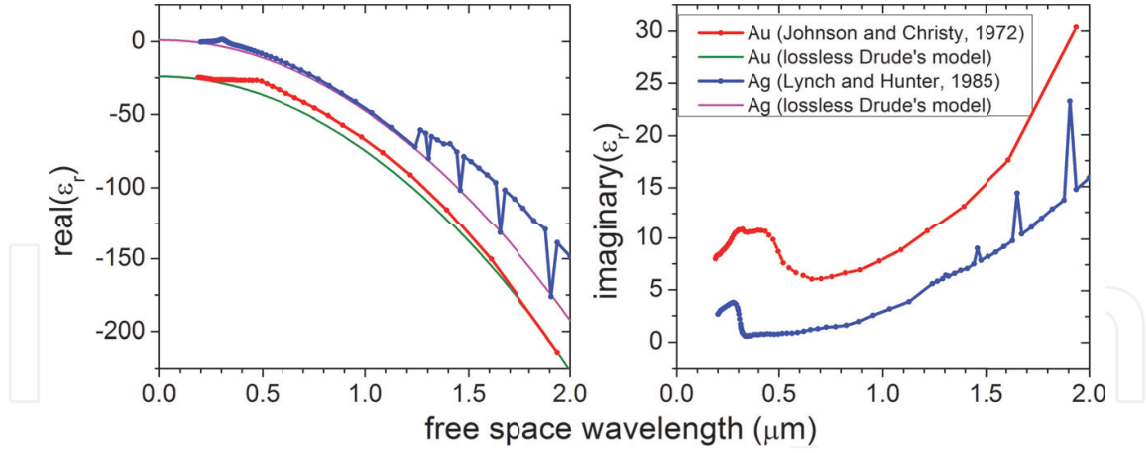
Figure 1. Permittivities of metals. Silver is modelled by the Drude's model without damping ($\omega_p = 13.1\,\text{Prad}$, $\lambda_p = 144\,\text{nm}$) and the tabulated values of Lynch and Hunter (1985) [20]. Gold is modelled by the Drude's model without damping ($\omega_p = 13.4\,\text{Prad}$, $\lambda_p = 141\,\text{nm}$) and the tabulated values of Johnson and Christy (1972) [13]. For easiness of visualisation, the real part of gold permittivity was shifted -25 units, and the imaginary part, $+5$ units.

Thus a field can be described by a vector phasor $\vec{F}(\vec{r})$, which contains information on the magnitude, direction and phase [3].

In plasmonics, it is common to deal with structures without any external current sources and/or charges. In this situation, we apply the source-free macroscopic Maxwell's equations, in which the displacement charges and currents are fully incorporated in the permittivities and permeabilities of the materials.

In the time-harmonic regime, the source-free macroscopic Maxwell's equations can be written as [3]

$$
\begin{aligned}
\text{Gauss' law of electricity:} \quad & \vec{\nabla} \cdot \vec{D}(\vec{r}) = 0 \\
\text{Gauss' law of magnetism:} \quad & \vec{\nabla} \cdot \vec{B}(\vec{r}) = 0 \\
\text{Faraday's law of induction:} \quad & \vec{\nabla} \times \vec{E}(\vec{r}) = i\omega \vec{B}(\vec{r}) \\
\text{Ampère's circuital law:} \quad & \vec{\nabla} \times \vec{H}(\vec{r}) = -i\omega \vec{D}(\vec{r})
\end{aligned}
\tag{4}
$$

3.2. Boundary conditions

The source-free Maxwell's equations in their integral form applied to the interface between two different media (1 and 2) lead to four boundary conditions [10, 29]:

$$
\begin{aligned}
\hat{n} \cdot \left(\vec{D}_2 - \vec{D}_1 \right) &= 0 \\
\hat{n} \cdot \left(\vec{B}_2 - \vec{B}_1 \right) &= 0 \\
\hat{n} \times \left(\vec{E}_2 - \vec{E}_1 \right) &= 0 \\
\hat{n} \times \left(\vec{H}_2 - \vec{H}_1 \right) &= 0
\end{aligned}
\tag{5}
$$

These boundary conditions describe the continuity of the components of the fields perpendicular and parallel to the interface. Moreover, the momentum parallel to the interface

is also continuous [12]. In such case, one can write the boundary conditions as

$$\vec{D}_{2\perp} = \vec{D}_{1\perp} \tag{6a}$$

$$\vec{B}_{2\perp} = \vec{B}_{1\perp} \tag{6b}$$

$$\vec{E}_{2\parallel} = \vec{E}_{1\parallel} \tag{6c}$$

$$\vec{H}_{2\parallel} = \vec{H}_{1\parallel} \tag{6d}$$

$$\vec{k}_{2\parallel} = \vec{k}_{1\parallel} \tag{6e}$$

3.3. Electromagnetic waves

The Maxwell's equations represent a coupled system of differential equations. With some algebraic manipulation, it is possible to transform these four equations (4) into two uncoupled ones, representing the homogeneous vector wave equations for the electric and magnetic fields. In the time-harmonic regime, these wave equations become the homogeneous vector Helmholtz' equations [3]:

$$\nabla^2 \vec{E} + k^2 \vec{E} = 0$$
$$\nabla^2 \vec{H} + k^2 \vec{H} = 0 \tag{7}$$

In which

$$k = \frac{\omega}{v} = nk_0 = \sqrt{\mu\varepsilon}k_0 \tag{8}$$

is the wavenumber in a medium with index of refraction $n = \sqrt{\mu\varepsilon}$, and $k_0 = \omega/c$ is the free-space wavenumber.

3.4. Light polarisation

Due to the linearity of the homogeneous Helmholtz' equations, we can divide the problem of a wave incident to a planar surface into two parts: for an s- and for a p-polarised wave[2]. These waves are depicted in Figure 2, in which we define the plane of incidence as the *x-z* plane.

In these conditions, for a plane wave propagating in the *x-z* plane, the magnitudes of the phasor fields are dependent on the coordinates *x* and *z*, but constant along the *y* direction. In order to find the surface plasmons — which are waves bound to the interfaces —, we can write the magnitudes of the electric and magnetic phasor fields as

$$\vec{E}(\vec{r}) = \vec{E}(x,z) = \vec{E}(z)\,e^{i\beta x}$$
$$\vec{H}(\vec{r}) = \vec{H}(x,z) = \vec{H}(z)\,e^{i\beta x} \tag{9}$$

Where β is the propagation constant, in the *x* direction. As the parallel wavevector to the interface must be constant (Eq. 6e), we have

$$\beta = k_{x,1} = k_{x,2} \tag{10}$$

---

[2] The terms s- and p-polarised are the initials of the German words: *senkrecht* (perpendicular) and *parallel*. In this nomenclature, s or p means that the electric field is perpendicular (s) or parallel (p) to the plane of incidence [23]. The s-polarisation is also called TE (transverse electric); and the p-polarisation, TM (transverse magnetic) [3, 29].
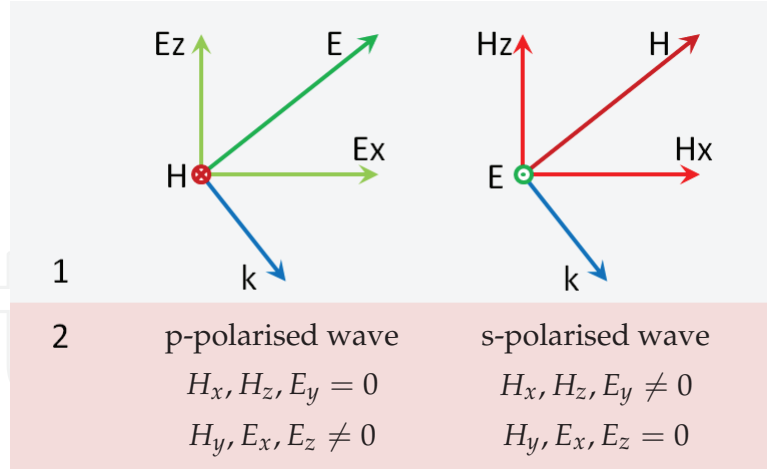
Figure 2. Interface between two media (1 and 2), showing the polarisation vectors of a p-polarised (left) and an s-polarised waves (right). The plane of incidence coincides with the page. A p-polarised wave (TM) is characterised by the magnetic field perpendicular to the plane of incidence; while an s-polarised (TE) wave is characterised by the electric field perpendicular to the plane of incidence.

In this case, the differential operators with respect to the coordinates x and y can be written as

$$\frac{\partial}{\partial x} = i\beta$$
$$\frac{\partial}{\partial y} = 0 \tag{11}$$

This makes it possible to express the divergence and Laplacian of any of the fields as

$$\vec{\nabla} \times \vec{F}(x,z) = \begin{vmatrix} e_x & e_y & e_z \\ i\beta & 0 & \frac{\partial}{\partial z} \\ F_x & F_y & F_z \end{vmatrix} = \left(-\frac{\partial F_y}{\partial z}\right)\hat{e}_x + \left(\frac{\partial F_x}{\partial z} - i\beta F_z\right)\hat{e}_y + \left(i\beta F_y\right)\hat{e}_z \tag{12a}$$

$$\nabla^2 \vec{F}(x,z) = \frac{\partial^2 \vec{F}}{\partial z^2}(x,z) - \beta^2 \vec{F}(x,z) \tag{12b}$$

3.4.1. Revisiting Helmholtz' equations and boundary conditions

The Laplacian in Equation 12b and the fields in Equation 9 can be used to simplify the Helmholtz' equations (7) to one dimension [21]:

$$\frac{\partial^2 \vec{E}}{\partial z^2}(z) - \gamma_z^2 \vec{E}(z) = 0 \tag{13a}$$

$$\frac{\partial^2 \vec{H}}{\partial z^2}(z) - \gamma_z^2 \vec{H}(z) = 0 \tag{13b}$$

With

$$\gamma_j^2 = -k_{z,j}^2 = \beta^2 - \varepsilon_j k_0^2 \tag{14}$$

$k_{z,j}$ is the wavevector along the z axis in the medium j $(= 1, 2)$. We define the propagation constant γ as

$$\gamma = ik_z \tag{15}$$

This definition is commonly done in transmission-line theory [3], and it is also used in most of the literature about PSPs. We note that, when dealing with a theoretical situation of lossless materials, working with γ implies in dealing with real numbers instead of imaginary.

It is sufficient to solve one of the Helmholtz' equation for the polarisation whose field (electric or magnetic) is perpendicular to the plane of incidence (Figure 2). In other words, for the s-polarised wave, whose electric field has only the y-component, we solve Equation 13a; while for the p-polarised wave, whose magnetic field has only the y-component, we solve Equation 13b.

The Helmholtz' equations are differential equations of second order, and each one needs two boundary conditions in order to be solved. Equations 6c and 6d, describing the continuity of the parallel electric and parallel magnetic fields, provide one boundary condition for each of the Helmholtz' equations. Below, we provide one additional boundary condition for each field (electric and magnetic).

3.4.2. s-polarisation

Expanding the divergence (Equation 12a) in the Faraday's law (Equation 4) for an s-polarised wave (Figure 2), we get

$$\left(-\frac{\partial E_y}{\partial z}\right)\hat{e}_x + \left(i\beta E_y\right)\hat{e}_z = \left(i\omega B_x\right)\hat{e}_x + \left(i\omega B_z\right)\hat{e}_z \tag{16}$$

- **z component**: The continuity of the perpendicular $\vec{B}$ field (Equation 6b), B_z, implies the continuity of βE_y. As β is continuous (Equation 10), this condition is equivalent to the previous condition of continuity of E_y (Equation 6c).

- **x component**: For homogeneous isotropic materials, $\vec{B} = \mu\vec{H}$. Therefore,

$$i\omega H_x = -\frac{1}{\mu}\frac{\partial E_y}{\partial z} \tag{17}$$

This equation, together with the continuity of the parallel magnetic field (Equation 6d), leads to the continuity of $\frac{1}{\mu}\frac{\partial E_y}{\partial z}$.

In summary, the conditions for the s-polarised wave are:

$$\text{Continuity conditions for s-polarised wave:} \quad \begin{aligned} E_{y,1} &= E_{y,2} \\ \frac{1}{\mu_1}\frac{\partial E_{y,1}}{\partial z} &= \frac{1}{\mu_2}\frac{\partial E_{y,2}}{\partial z} \end{aligned} \tag{18}$$

3.4.3. p-polarisation

For the p-polarised wave, we use the same approach as for the s-polarised one. Expanding the divergence (Equation 12a), in the Ampère's law (Equation 4), we obtain

$$\left(-\frac{\partial H_y}{\partial z}\right)\hat{e}_x + \left(i\beta H_y\right)\hat{e}_z = -\left(i\omega D_x\right)\hat{e}_x - \left(i\omega D_z\right)\hat{e}_z \tag{19}$$

- **z component**: The continuity of the perpendicular $\vec{D}$ field (Equation 6a), D_z, implies the continuity of βH_y. As β is continuous (Equation 10), this condition is equivalent to the previous condition of continuity of H_y (Equation 6d).

- **x component**: For homogeneous isotropic materials, $\vec{D} = \varepsilon \vec{E}$. Therefore,

$$i\omega E_x = \frac{1}{\varepsilon} \frac{\partial H_y}{\partial z}. \tag{20}$$

This equation together with the continuity of the parallel electric field (Equation 6c) leads to the continuity of $\frac{1}{\varepsilon} \frac{\partial H_y}{\partial z}$ [2].

In summary, the conditions for the p-polarised wave are:

$$\text{Continuity conditions for p-polarised wave:} \quad \begin{aligned} H_{y,1} &= H_{y,2} \\ \frac{1}{\varepsilon_1} \frac{\partial H_{y,1}}{\partial z} &= \frac{1}{\varepsilon_2} \frac{\partial H_{y,2}}{\partial z} \end{aligned} \tag{21}$$

4. PSP at a planar interface

Now we discuss the conditions satisfied by a wave propagating at a planar interface between two half-spaces. So as to solve the problem of an s-polarised wave propagating at an interface, we will use Equation 13a, and the two boundary conditions stated in Equations 18. For the p-polarised wave, we will use Equation 13b and the boundary conditions in Equations 21.

4.1. s-polarised wave

In order to solve Equation 13a, we postulate a solution of a certain form, and verify that it indeed satisfies our equation and boundary conditions. We are looking for a wave bound to the interface, that vanishes away from it. With this in mind, and inspecting Equation 13a, we postulate our solution to be

$$\vec{E}(z) = \begin{cases} E_1 e^{-\gamma_1 z} \hat{e}_y, & z > 0 \\ E_2 e^{\gamma_2 z} \hat{e}_y, & z < 0 \end{cases} \tag{22}$$

with the real parts of γ_j positive in order to have a field decaying away from the interface. Applying the boundary conditions to this ansatz, we find

$$\begin{aligned} E_1 &= E_2 \\ \frac{\gamma_1}{\mu_1} E_1 &= -\frac{\gamma_2}{\mu_2} E_2 \end{aligned} \tag{23}$$

These conditions are equivalent to [27]

$$\frac{\gamma_1}{\mu_1} = -\frac{\gamma_2}{\mu_2} \tag{24}$$

For the materials found in nature, the permeability at optical frequencies is close to unity[3] [27]. This leads to $\gamma_1 = -\gamma_2$, what is impossible as the real components of both γ_1 and γ_2 are

---

[3] The relative permeability of unity in the optical regime for most of the materials implies that the index of refraction is $n = \sqrt{\varepsilon\mu} = \sqrt{\varepsilon}$.

positive. However, magnetic surface plasmons can be achieved by the use of metamaterials [24], for which the magnetic permeability can be engineered to be negative at frequencies higher than in natural materials. For example, ref. [19] shows magnetic plasmon propagation at infra-red along a chain of split-ring resonators.

4.2. p-polarised wave

Similarly to the case of an s-polarised wave, we propose the following solution for the Equation 13b:

$$\vec{H}(z) = \begin{cases} H_1 e^{-\gamma_1 z} \hat{e}_y, & z > 0 \\ H_2 e^{\gamma_2 z} \hat{e}_y, & z < 0 \end{cases} \tag{25}$$

Applying the boundary conditions:

$$\begin{aligned} H_1 &= H_2 \, (= H_0) \\ \frac{\gamma_1}{\varepsilon_1} H_1 &= -\frac{\gamma_2}{\varepsilon_2} H_2 \end{aligned} \tag{26}$$

These conditions lead to [7, 21, 23, 27, 28, 34]

$$\frac{\gamma_1}{\varepsilon_1} = -\frac{\gamma_2}{\varepsilon_2} \tag{27}$$

This condition combined with Equation 14 and the index of refraction[3] $n = \sqrt{\varepsilon}$ leads to the dispersion relation[4] [4, 7, 21, 23, 34]:

$$\text{Dispersion relation for half-spaces:} \quad \beta^2 = k_0^2 \frac{\varepsilon_1 \varepsilon_2}{\varepsilon_1 + \varepsilon_2} \tag{28}$$

Substituting this β^2 in Equation 14, one obtains the normal component of the wavevector [4, 23]:

$$k_{z,j}^2 = -\gamma_j^2 = k_0^2 \frac{\varepsilon_j^2}{\varepsilon_1 + \varepsilon_2} \tag{29}$$

4.2.1. Conditions for PSPs

In this subsection, we limit our discussion on the conditions for the existence of PSPs to lossless materials. Subsequently, we will discuss the effect of complex permittivities on β and γ. In lossless materials, all permittivities as well as the propagation constants (Equations 28 and 29) are real. Without loss of generality, one can define the surface wave propagating at the direction $+x$. Hence, β is positive (Equation 28). 1) This requires that $\varepsilon_1 \varepsilon_2$ and $\varepsilon_1 + \varepsilon_2$ are both positive or both negative. Furthermore, as we are looking for the modes bound to the interface, we want the field propagating at the boundary, but not along the z axis. Therefore, γ must be positive real (Equation 25) (or $k_{z,1}$ and $k_{z,2}$ must be positive imaginary, Equation 15), leading to evanescent, exponentially decaying fields away from the interface. 2) This requirement is achievable only if $\varepsilon_1 + \varepsilon_2$ is negative (Equation 29). As a result, the conditions for the existence of PSPs are [23]

---

[4] The dispersion relation is an equation that relates the wavevector along the direction of propagation and the frequency.

$$\text{Conditions for PSPs:} \quad \begin{array}{l} \varepsilon_1 \varepsilon_2 < 0 \\ \varepsilon_1 + \varepsilon_2 < 0 \end{array} \tag{30}$$

The first condition states that one of the permittivities must be positive, and the other one, negative. The second condition, indicates that the absolute value of the negative permittivity must be higher than the positive one [23].

As already seen in Figure 1 and Equation 2, lossless Drude's metals have negative permittivities for $\omega < \omega_p$ (or $\lambda > \lambda_p$). The absolute values of these permittivities increase with the wavelength, exceeding the values found in dielectrics. Semiconductors [26] and graphene [9, 25] have also been used for their plasmonic properties in the terahertz range. Although in graphene there is no strict surface plasmon, due to its two-dimensional geometry, which practically prevents transverse oscillations of electrons [11]. As metals are the most common materials used for PSPs, a planar interface that supports bound waves will henceforth be called insulator-metal (IM) geometry.

Other important consideration to take into account, when calculating the wavevectors, is the position of β in relation to the light line. If β is at right of the light line ($\beta^2 > \varepsilon_j k_0^2$) (Equation 14) in the medium j, γ_j is real ($k_{z,j}$ is imaginary). If β is at left ($\beta^2 < \varepsilon_j k_0^2$), γ is imaginary ($k_{z,j}$ is real), leading to the propagation of the wave away from the interface [2].

4.2.2. Complex β and γ in lossy materials

When the permittivity of any medium in the structure is complex, the normal and perpendicular wavevectors components are complex. The magnetic field (Equations 9 and 25) can be re-written in the following form:

$$\vec{H}(\vec{r}) = \vec{H}(z) e^{i\beta x} = \begin{cases} H_0 e^{i\beta x} e^{-\gamma_1 z} \hat{e}_y, & z > 0 \\ H_0 e^{i\beta x} e^{\gamma_2 z} \hat{e}_y, & z < 0 \end{cases} \tag{31}$$

At the interface ($z = 0$), this converges to

$$\vec{H}(x, y, 0) = H_0 e^{i\beta x} \hat{e}_y = H_0 e^{iRe(\beta)x} e^{-Im(\beta)x} \hat{e}_y \tag{32}$$

Looking at this equation, we remind that the meaning of the (positive) real part of β is that the wave propagates on the interface towards $+x$. If the imaginary part of β is negative, the field increases exponentially (Equation 32), which is un-physical in our situation. Consequently, the imaginary part of β must be positive, leading to an exponential decay with x. Lossless materials ($Im(\beta = 0)$) imply an endless propagation of the PSP along the interface. One can define the propagation length as the distance the wave travels along the interface until its energy decays to e^{-1} (≈ 0.368) of its original value. As the energy is proportional to the square of the field ($energy \propto |H|^2 \propto e^{-2Im(\beta)x}$), the propagation length is [7, 21, 34]

$$propagation\ length \equiv L_{sp} = \frac{1}{2Im(\beta)} \tag{33}$$

Now we analyse the component of the wavevector that is perpendicular to the interface, γ_j. For a fixed x, Equation 31 can be re-written as

$$\vec{H}(constant, y, z) = H_0 e^{i\beta x} \times \begin{cases} e^{-Re(\gamma_1)z} e^{-iIm(\gamma_1)z} \hat{e}_y, & z > 0 \\ e^{Re(\gamma_2)z} e^{iIm(\gamma_2)z} \hat{e}_y, & z < 0 \end{cases} \tag{34}$$

For bound modes, we remind that $Re(\gamma_j)$ must be positive (or $Im(k_{z,j})$ must be negative). Equation 14 tells γ has two solutions in anti-phase in the complex plane. One must choose, therefore, the solutions in the first and fourth quadrants.

4.2.3. Dispersion curve

Applying the lossless Drude's model (Equation 2) to the dispersion relation for the IM geometry (Equation 28), one obtains the result presented in Figure 3A. In this figure, we plotted the solution for two different dielectrics: free-space and a material with $n = 1.5$ throughout the entire spectral range. The dispersion is divided into two branches with a region between them where β is imaginary. In this region, called plasmon bandgap [4], the wave is evanescent and it reflects back to the dielectric. For the Drude's model without damping (Equation 2), the index of refraction of a metal is real when the angular frequency is larger than the plasma frequency ($\omega > \omega_p$). Therefore, the material is transparent and the wave propagates freely [12, 28]. This radiation mode is called Brewster mode [28]. Under the plasmon bandgap, there is a region limited by what is called the surface plasmon frequency, the frequency in which β diverges. It occurs when the permittivity of the metal (ε_m) cancels that one of the dielectric (ε_d) (Equation 28) [4, 21, 34]:

$$\varepsilon_m = -\varepsilon_d \Rightarrow \omega_{sp} = \frac{\omega_p}{\sqrt{1 + \varepsilon_d}} \tag{35}$$

The higher the index of refraction of the dielectric is, the lower the surface plasmon frequency is. From this frequency down, light propagates in a bound mode. For a very high wavevector[5], the electric field has an electrostatic character, as the wavelength along the interface ($= 2\pi/\beta$) tends to zero. Likewise, the group velocity ($d\omega/dk$) [21] and the decay lengths into the metal and dielectric ($= 1/Re(\gamma_j)$) tend to zero. This high confinement of light at the interface indicates a true surface mode, called Fano mode [28]. For very low frequencies, the dispersion converges to the light line, in a regime called Sommerfeld-Zenneck waves [21, 28].

Using the complex experimental values of permittivity, the dispersion relation (Equation 28) is shown is Figure 3B. As the metal is no longer modelled as lossless, β is complex, leading to a finite propagation length (Equation 33), drawn in Figure 3C. Here, the wavenumber does not diverge as previously. It bends backwards filling the region previously called plasmon bandgap and connects to the Brewster mode. This region of anomalous dispersion (negative phase velocities $= d\omega/dk$) is called quasi-bound mode [4].

In the infra-red, the imaginary part of the permittivity of silver is very small compared to the real part. As a consequence, the propagation length is around 10–1000 μm. In the region of the quasi-bound mode, the imaginary component reaches values comparable to the real component (up to 0.83 of the real part for n=1, up to 1.9 for n=1.5), leading to a decrease in the propagation length down to 10–100 nm.

5. Physical interpretation

An electromagnetic wave inside a material induces polarisation in the medium. The coupled excitation resulting from the interaction between an incident electromagnetic wave and the

---

[5] In surface plasmons, the wavevector is higher than it would be in the dielectric, leading to a wavelength shorter than the one in the dielectric. This has applications in super-resolution light microscopy [15, 33].
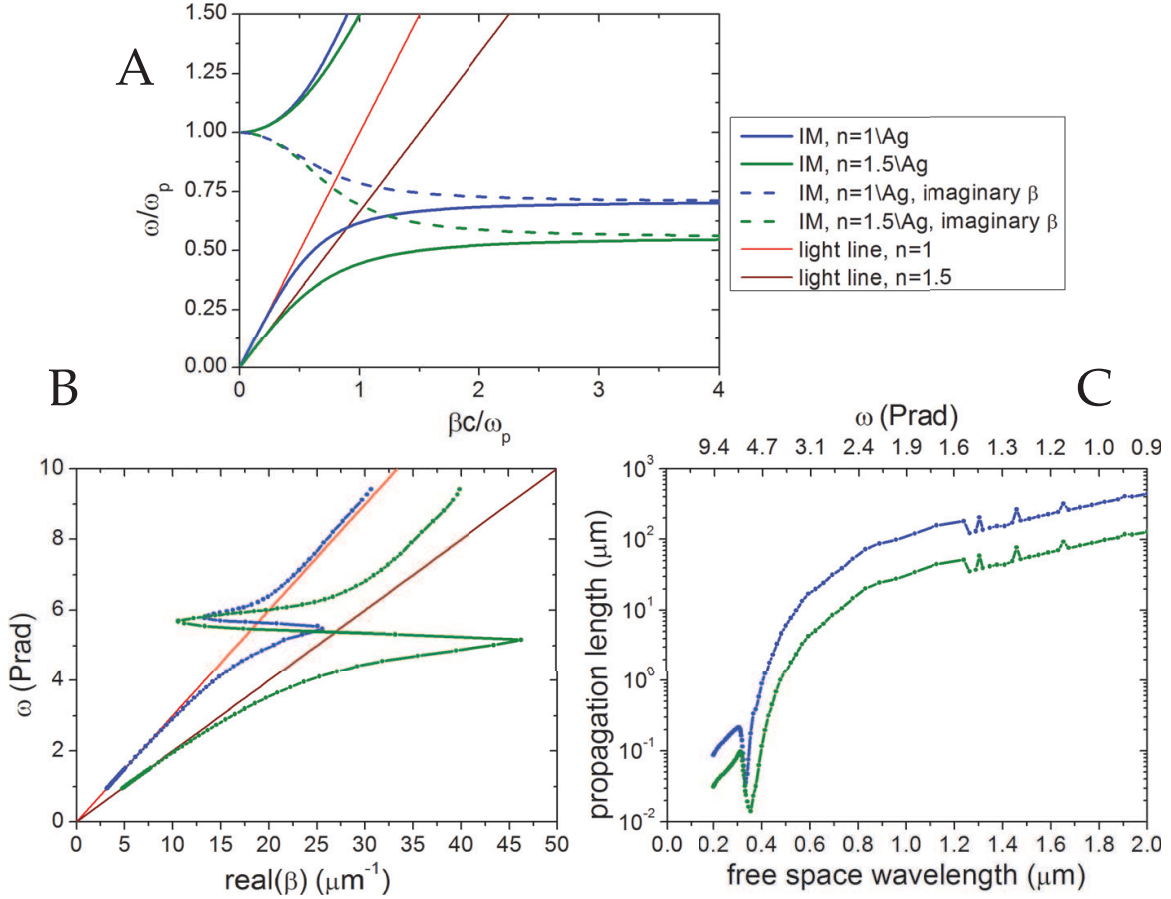
Figure 3. Dispersion curve and propagation length (Equation 28) for PSPs on an interface between half-spaces of a metal and insulators with refractive indices of 1 or 1.5. A) Drude's metal without damping. The imaginary β in the bandgap is also shown. B) Dispersion curve and C) propagation length for tabulated values of the metal (silver) permittivity.

material polarisation is called polariton [22, 31]. The way the coupling occurs is responsible for permittivity, permeability and light velocity being different from those ones in vacuum [22]. When the polariton is restricted to a small region around an interface, it is called surface polariton [31]. There are diverse types of polaritons according to the induced excitation, such as phonon-polariton [8], exciton-polariton [30], plasmon-polariton etc. The latter is the interest in the context of PSPs.

Plasmon is technically a quantum of charge density oscillation in a plasma [18]. The plasmons can be divided into two main types: bulk plasmons — arising from fluctuations of the free charge density inside the material which propagate as a longitudinally-polarised charge-density wave [18] — and surface plasmons (SPs) — which propagate along the interfaces of materials under specific circumstances. The SPs can be subdivided in localised surface plasmons (LSPs) and propagating surface plasmons (PSPs). In the former, the charge oscillations are confined to a nanostructure; while in the latter, the charge oscillation propagates relatively large distances, from tens of nanometers to hundreds of micrometers (Figure 3C).

We showed in the previous section that electromagnetic waves can propagate along the interfaces between dielectrics and metals. In response to an incidence electric field, the

electrons of the metal induce an opposing field determined by the dielectric function of the metal. The fact that in metals the charge density is confined to a small region close to the surface, leads to high enhancement of the electric field, which can be as high as about 100 times[6] [27].

6. Exciting PSPs

As demonstrated previously, the wavenumber of a PSP is higher than the wavenumber in the dielectric (Figure 3A and B). Hence, light incident at an IM interface typically cannot excite PSPs. In order to do so, it is necessary to artificially increase the wavenumber of the light, so that the wavevectors in both materials can be matched. Some of the techniques to excite PSPs include the Otto and Kretschmann configurations, and the application of a grating or other periodic structure.

The Otto and Kretschmann configurations [7, 23, 27, 34] relies on the proximity of a dielectric with a higher index of refraction than the dielectric of the interface where the PSP is being excited. As the wavenumber is directly proportional to the index of refraction (Equation 8), one can use the evanescent waves that arise from a total internal reflection on a high-refractive index material to excite PSPs. In the Otto configuration, the reflectance comes from the side of the interface dielectric; while in the Kretschmann one, the evanescent waves come across a thin metal layer to excite the interface on the other side.

Diffraction gratings provide light with an additional momentum on the grating axis due to the spatial periodicity, allowing the coupling of light to PSPs [7, 27]. For a one-dimensional lattice, the additional momentum is given by

$$\Delta k = m\frac{2\pi}{a} \tag{36}$$

Where a is the period of the grating, and m is an integer.

7. PSP at a thin layer

The actual geometry of a thin layer (medium 2) between two media (1 and 3) is presented in Figure 4A. As previously discussed for an IM geometry, only p-polarised wave can excite PSP in naturally-occurring materials. This statement is also valid for other geometries. In a p-polarised wave, there is an electric field perpendicular to the surface (Figure 2). As D_z is continuous (Equation 6a), E_z changes, resulting in the creation of charge density at the interface. In an s-polarised wave, the electric field has no component parallel to the surface, therefore it is continuous and it does not produce charge density at the surface [14]. For modes bound to the interface in p-polarisation, we postulate the magnetic field — stronger at the interface and exponentially decaying away from it — as

$$H_y\left(z\right) = \begin{cases} H_1 e^{-\gamma_1 z}, & z > \frac{a}{2} \\ H_2^- e^{-\gamma_2 z} + H_2^+ e^{\gamma_2 z}, & \frac{a}{2} > z > -\frac{a}{2} \\ H_3 e^{\gamma_3 z}, & -\frac{a}{2} > z \end{cases} \tag{37}$$

Applying the continuity conditions (Equations 21) to the ansatz given in Equation 37, we

---

[6] This enhancement of the electric field may be applied for surface-enhanced spectroscopies, such as surface-enhanced Raman spectroscopy (SERS), surface-enhanced fluorescence (SEF) [17] and surface-enhanced infra-red absorption (SEIRA) [1].
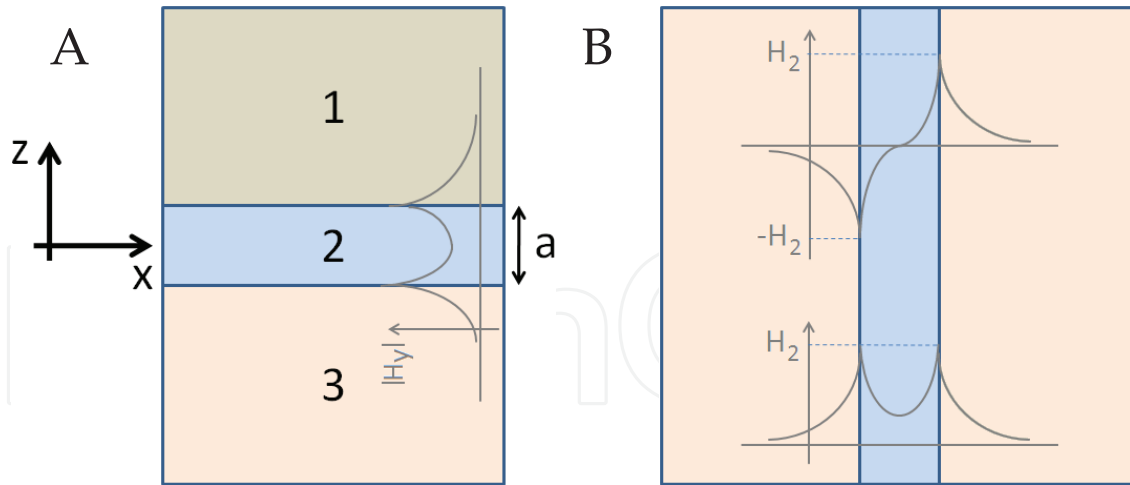
Figure 4. Planar thin layer geometry. A) Geometry of a planar thin layer surrounded by two half-spaces. It also shows the absolute value of the magnetic field expected for modes bound to the interfaces. B) The field magnitudes for the symmetric and anti-symmetric PSPs in a symmetric thin layer.

obtain four equations, two for each boundary.

- Boundary 1–2 ($z = a/2$)

$$H_1 e^{-\gamma_1 a/2} = H_2^- e^{-\gamma_2 a/2} + H_2^+ e^{\gamma_2 a/2} \tag{38}$$

$$\frac{\gamma_1}{\varepsilon_1} H_1 e^{-\gamma_1 a/2} = \frac{\gamma_2}{\varepsilon_2} H_2^- e^{-\gamma_2 a/2} - \frac{\gamma_2}{\varepsilon_2} H_2^+ e^{\gamma_2 a/2} \tag{39}$$

- Boundary 2–3 ($z = -a/2$)

$$H_3 e^{-\gamma_3 a/2} = H_2^- e^{\gamma_2 a/2} + H_2^+ e^{-\gamma_2 a/2} \tag{40}$$

$$\frac{\gamma_3}{\varepsilon_3} H_3 e^{-\gamma_3 a/2} = -\frac{\gamma_2}{\varepsilon_2} H_2^- e^{\gamma_2 a/2} + \frac{\gamma_2}{\varepsilon_2} H_2^+ e^{-\gamma_2 a/2} \tag{41}$$

To simplify the notation, we define

$$R_i = \frac{\gamma_i}{\varepsilon_i} \tag{42}$$

Substituting $H_1 e^{-\gamma_1 a/2}$ in Equation 39 by 38, $H_3 e^{-\gamma_3 a/2}$ in 41 by 40, and multiplying by $e^{\gamma_2 a/2}$, we obtain

$$R_1 \left(H_2^- + H_2^+ e^{\gamma_2 a} \right) = R_2 \left(H_2^- - H_2^+ e^{\gamma_2 a} \right) \tag{43}$$

$$R_3 \left(H_2^+ + H_2^- e^{\gamma_2 a} \right) = R_2 \left(H_2^+ - H_2^- e^{\gamma_2 a} \right) \tag{44}$$

The original system of four variables is now reduced to two: H_2^+ and H_2^-. Re-arranging the terms, we can obtain the following relationship in a matrix form:

$$\begin{pmatrix} e^{\gamma_2 a} (R_1 + R_2) & R_1 - R_2 \\ R_3 - R_2 & e^{\gamma_2 a} (R_2 + R_3) \end{pmatrix} \begin{pmatrix} H_2^+ \\ H_2^- \end{pmatrix} = \begin{pmatrix} 0 \\ 0 \end{pmatrix} \tag{45}$$

This is a homogeneous system of linear equations. Its non-zero solutions occur when the determinant of the matrix of coefficients is zero, resulting in [21]

$$\text{Dispersion relation for thin layer:} \quad e^{2\gamma_2 a} = \frac{R_1 - R_2}{R_1 + R_2} \frac{R_3 - R_2}{R_3 + R_2} \tag{46}$$

γ_2 and R_i are given by Equations 14 and 42, respectively.

7.1. Symmetric structures

Suppose that media 1 and 3 are composed of the same material. In this case, the dispersion relation (Equation 46) becomes

$$e^{2\gamma_2 a} = \left(\frac{R_1 - R_2}{R_1 + R_2} \right)^2 \tag{47}$$

This equation has two roots [28]:

$$e^{\gamma_2 a} = \pm \frac{R_1 - R_2}{R_1 + R_2} \tag{48}$$

Which can be re-arranged to

$$\frac{R_1}{R_2} = -\frac{e^{\gamma_2 a} \pm 1}{e^{\gamma_2 a} \mp 1} = -\frac{e^{\gamma_2 a/2} \pm e^{-\gamma_2 a/2}}{e^{\gamma_2 a/2} \mp e^{-\gamma_2 a/2}} \tag{49}$$

Or [21]

$$\frac{R_1}{R_2} = \begin{cases} -coth\left(\frac{\gamma_2 a}{2} \right) \\ -tanh\left(\frac{\gamma_2 a}{2} \right) \end{cases} \tag{50}$$

Returning to Equation 43 and re-arranging, we obtain

$$\frac{R_1}{R_2} = \frac{H_2^- - H_2^+ e^{\gamma_2 a}}{H_2^- + H_2^+ e^{\gamma_2 a}} = -\frac{e^{\gamma_2 a/2} - e^{-\gamma_2 a/2} \frac{H_2^-}{H_2^+}}{e^{\gamma_2 a/2} + e^{-\gamma_2 a/2} \frac{H_2^-}{H_2^+}} \tag{51}$$

Comparing Equations 50 and 51 leads to [4]

$$\text{Dispersion relation for symmetric thin layer:} \quad \begin{aligned} \frac{R1}{R2} &= -coth\left(\frac{\gamma_2 a}{2} \right) \Rightarrow H_2^+ = -H_2^- \\ \frac{R1}{R2} &= -tanh\left(\frac{\gamma_2 a}{2} \right) \Rightarrow H_2^+ = H_2^- \end{aligned} \tag{52}$$

Therefore, in symmetric structures, the PSPs has two branches: a symmetric (or even) and an anti-symmetric (or odd). A sketch of the field magnitude is shown in Figure 4B.

There are two possibilities for a symmetric structure: IMI (insulator-metal-insulator) and MIM (metal-insulator-metal). We will show in sequence the dispersion curves for the symmetric IMI, symmetric MIM and their respective asymmetric variants.

7.2. Dispersion curves for a thin layer

Applying lossless Drude's metal for the dispersion relation for symmetric IMI (Equations 52), we obtain the curves depicted in Figure 5A and B. In 5A, the metal is immersed in free space, while in 5B, it is immersed in a dielectric with $n = 1.5$. The dispersion curves of the light lines in the dielectrics and of the respective IM geometries are also plotted for comparison. In the thin layer case, the dispersion relationship splits in two modes. The even mode appears below the dispersion of the IM, while the odd mode appears above it. At very low frequencies, both

of the modes converge to the light line, as does the IM dispersion. For frequencies close to ω_{sp}, the wavevectors of both modes tend to infinity. The bulk mode appears only for the even mode, very similar to the one of the IM dispersion, but with higher wavevectors. The thinner is the layer, the farther the modes are from the IM dispersion. For thicker layers, the two modes converge to the IM dispersion [32], as expected due to lower interactions between the two interfaces. We note that more than one solution is possible for the odd mode, as shown in the inset in Figure 5A. Indeed, for the 25 nm layer, there were up to three solutions for each frequency.

For the symmetric MIM structures, the dispersion relation for a lossless Drude's metal is plotted in Figure 5C. The shape changes markedly from the IM dispersion. Now, the odd mode appears below the dispersion of the IM. This is the opposite of the result for the IMI geometry. Furthermore, the solution for the bulk mode appears only from the equation (52) of the odd mode. The even mode partially coincides with the plasmon bandgap, producing a quasi-bound mode. Close to ω_{sp}, the wavevectors of both modes tend to infinity. For very low frequencies, the odd mode does not tend to the light line as in the IMI structure. In addition, as expected, the thinner the layer is, the farther its dispersion is from the IM dispersion. The inset shows that, for the 50 nm layer, the even mode has two solutions for a range of frequencies.

The dispersion curve (Equation 46) for a 25 nm asymmetric IMI, is presented in Figure 5D. The mode that would be equivalent to the even mode in the symmetric variant appears under the IM dispersion with the high refractive-index dielectric. For very low frequencies, this mode converges to the light line of the same dielectric. The mode equivalent to the odd mode in the symmetric variant appears above the IM dispersion with the low refractive-index dielectric. Close to the respective ω_{sp}, the wavevector of this mode tends to infinity. For lower frequencies, there is a cut off. This mode disappears when it reaches the light line of the high refractive-index dielectric (see arrow in Figure 5D).

For a 25 nm asymmetric MIM (Figure 5E), the mode under the IM dispersions tends to infinity in the lower ω_{sp} (silver); while the mode above the IM dispersions tend to infinity in the higher ω_{sp} (gold). Silver has a lower plasma frequency than gold. Therefore, the IM dispersion of silver and vacuum remains under the IM dispersion of gold and vacuum. Between the ω_{sp} of the two half-spaces, there is a gap. In addition, the bulk mode also presents a cut-off frequency above the plasma frequencies of the two metals, when it reaches the IM dispersion of silver and vacuum (see arrow in Figure 5E).

The dispersion curves of the symmetric variants of IMI and MIM modelling the metals by the experimental values of permittivity are presented in Figure 6. As metals are modelled as lossy, the propagation lengths are also plotted. For the symmetric IMI with 25 and 50 nm lossy metal layer (Figure 6A and B), the odd modes are present in the entire frequency range. However, the even mode wavevectors of the IMI enters the bandgap region and decreases down to zero and re-appear in the bulk region. In the region of real surface plasmons, its wavevector is greater than the one of the odd mode. The odd mode, with smaller wavevectors, has propagation lengths longer than the lengths of the IM (Figure 6B), which — in its turn — are typically longer than the propagation length of the even mode. The even mode may have a longer propagation length only in the bulk mode, region not important for PSPs.

For the symmetric MIM structure with complex permittivities (Figure 6C and D), the even mode does not present a solution. At ω_{sp}, the odd mode wavevector is greater than the one in the IM dispersion. Its propagation length is shorter than the one of the IM case.
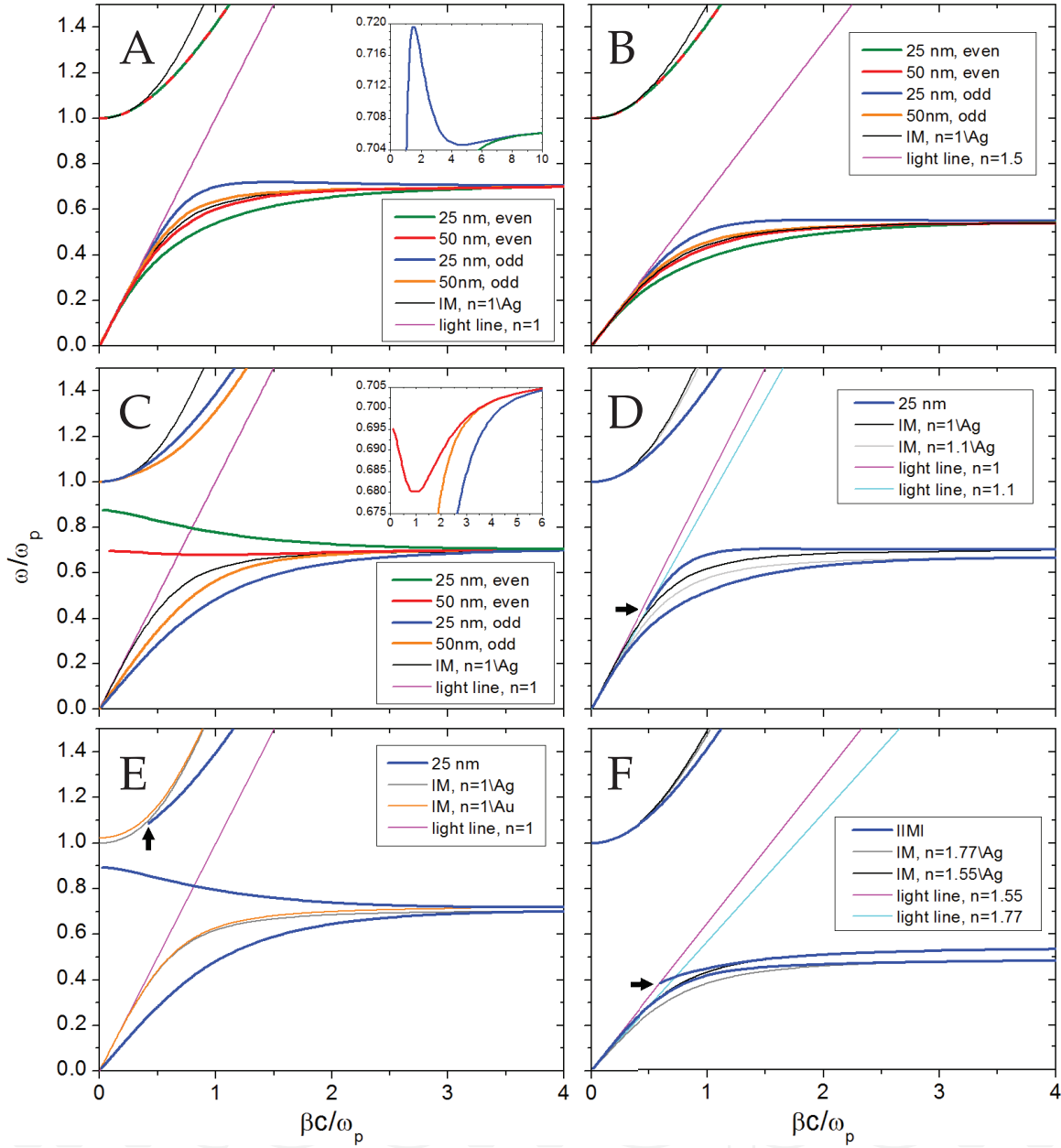
Figure 5. Dispersion relations for diverse geometries and lossless Drude's metals. A) Symmetric IMI: 25 and 50 nm metal layer immersed in free space. B) Similar to the previous geometry, but the metal is immersed in a dielectric with n=1.5. C) Symmetric MIM: 25 and 50 nm free-space layer immersed in metal. D) Asymmetric IMI: 25 nm metal layer surrounded by free space and other dielectric with n=1.1. E) Asymmetric MIM: 25 nm free space surrounded by silver and gold. F) IIMI: free space, 15 nm layer of a dielectric with n=1.77, 45 nm metal layer and a dielectric with n=1.55. The ω_p on the axes is the one of the silver. The insets in A and C show selected curves with different axes limits.
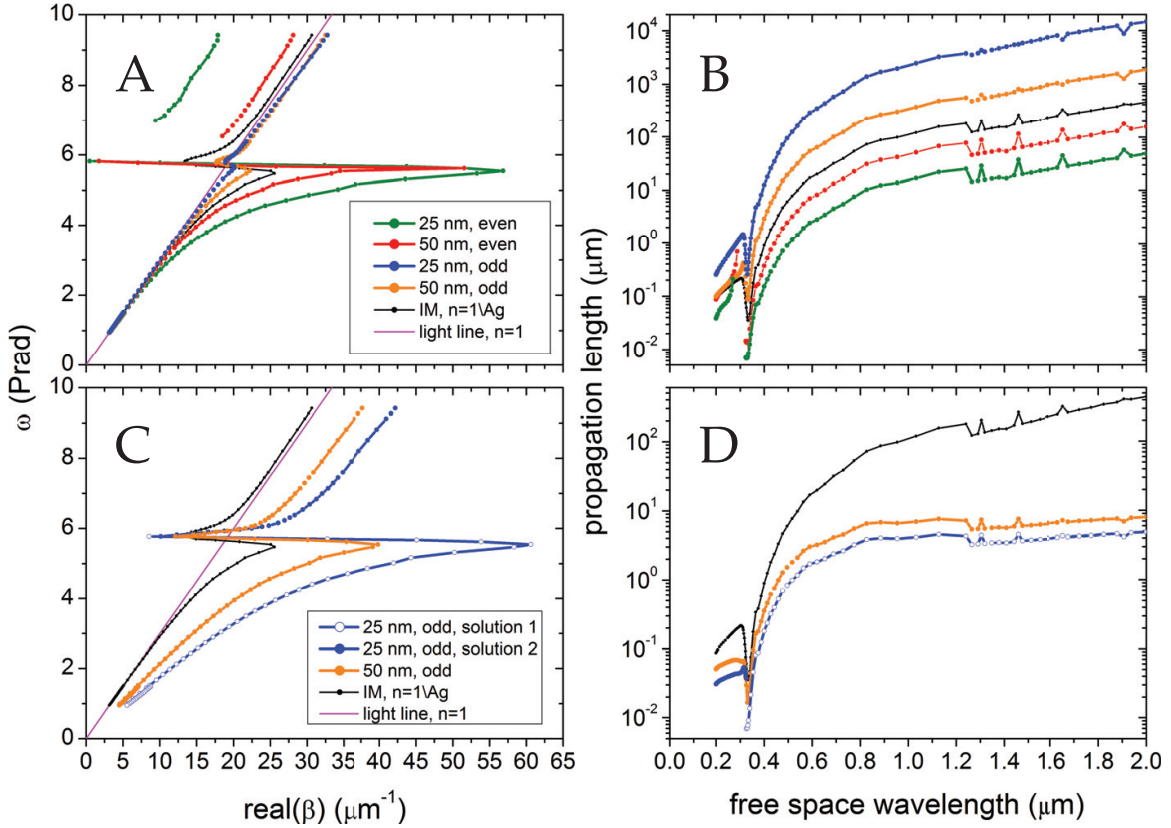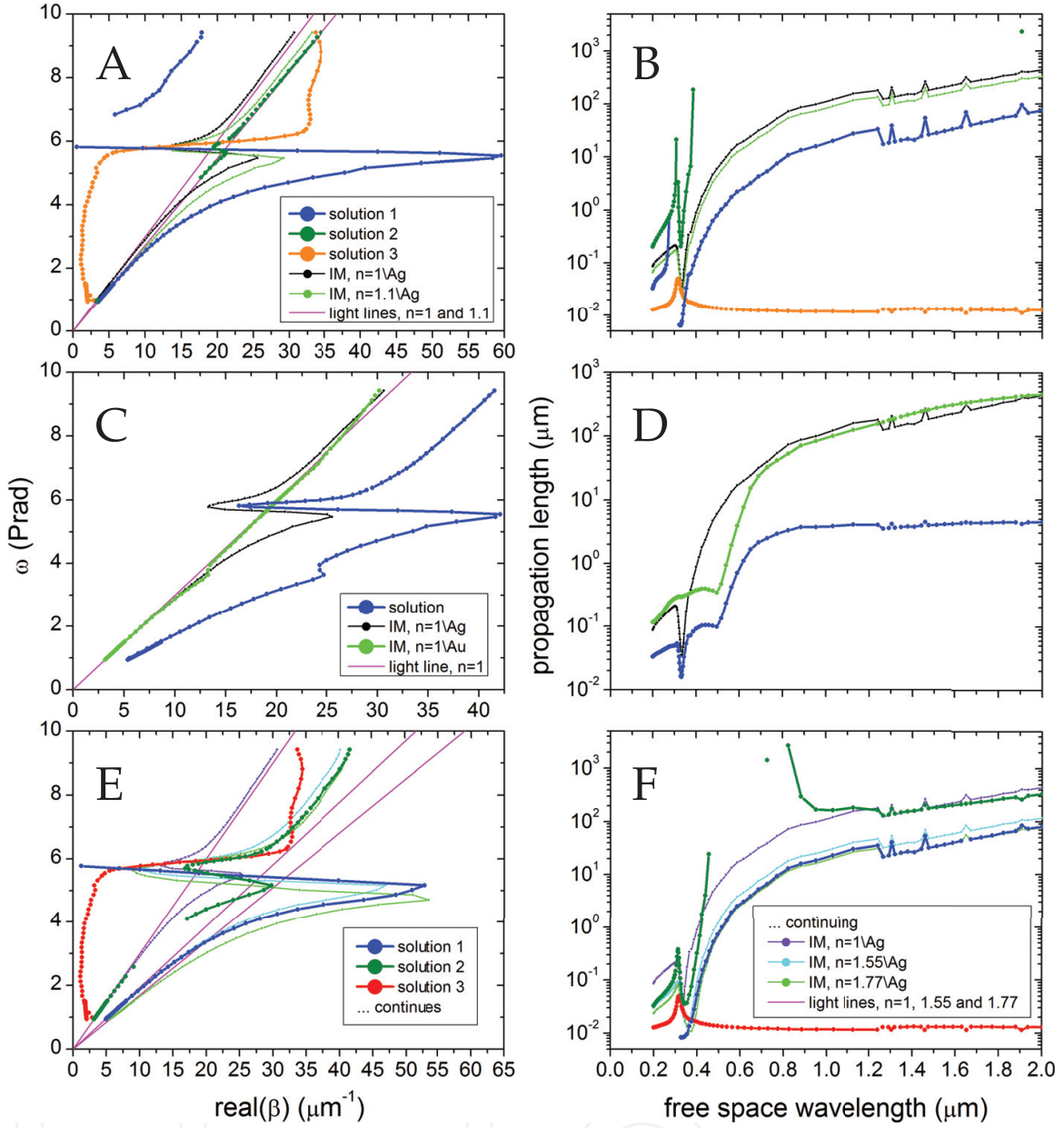
Figure 6. Dispersion curves and propagation lengths for symmetric geometries modelling the metals by the tabulated permittivities. A, B) IMI: 25 and 50 nm silver layer immersed in free space. C, D) MIM: 25 and 50 nm free-space layer immersed in silver.

The dispersion curves and propagation lengths of the asymmetric variants of IMI and MIM for tabulated permittivities are presented in Figure 7. For the IMI structure (Figure 7 A and B), instead of two solutions, three solutions appear. One of them (solution 3) has very short propagation length throughout the spectrum, and very low wavevector, except in the bulk region. Therefore, this mode does not produce PSP. The mode with great wavevector (solution 1), as the one in the symmetric case, enters the region of quasi-bond mode and decreases down to zero, with a bandgap, appearing again in the bulk region. Another mode (solution 2), with wavevectors close to the light line ($n = 1.1$), presented regions of cut-off in low frequencies as well as in the bulk region.

The MIM structure (Figure 7C and D) shows only one solution in the whole frequency spectrum. It is interesting to note that this solution presents two regions of PSPs, and consequently two quasi-bond mode regions. These regions corresponds to the ω_{sp} of the IM dispersion with silver and the ω_{sp} of the IM dispersion with gold. The propagation lengths are shorter than in any of the IM cases, with silver or with gold.

8. PSP at an IIMI structure

The geometry of an IIMI structure is depicted in Figure 8A. The structure consists of a thin metallic layer (m) deposited on a dielectric substrate (4), and covered by a thin dielectric layer (2) with free space on the top of the whole structure (1). The solution for the magnetic field of

Figure 7. Dispersion relations and propagation lengths for asymmetric geometries modelling the metals by the tabulated permittivities. A, B) IMI: 25 nm silver layer surrounded by free space and other dielectric with n=1.1. C, D) MIM: 25 nm free-space layer surrounded by silver and gold. E, F) IIMI: free space, 15 nm layer of a dielectric with n=1.77, 45 nm silver layer and a dielectric with n=1.55.

the p-polarised wave decaying away from the interfaces is postulated as

$$
H_y = e^{i\beta x} \times \begin{cases}
A_1 e^{-\gamma_1 z}, & a+b < z \\
A_2^- e^{-\gamma_2 z} + A_2^+ e^{\gamma_2 z}, & a < z < a+b \\
A_m^- e^{-\gamma_m z} + A_m^+ e^{\gamma_m z}, & 0 < z < a \\
A_4 e^{\gamma_4 z}, & z < 0
\end{cases}
\tag{53}
$$

One should not expect to have a PSP at the 1–2 interface, as both materials are dielectrics. Nevertheless, it is necessary to take into account evanescent waves decaying away from this interface. Otherwise, the IIMI structure would simply behave like an IMI.
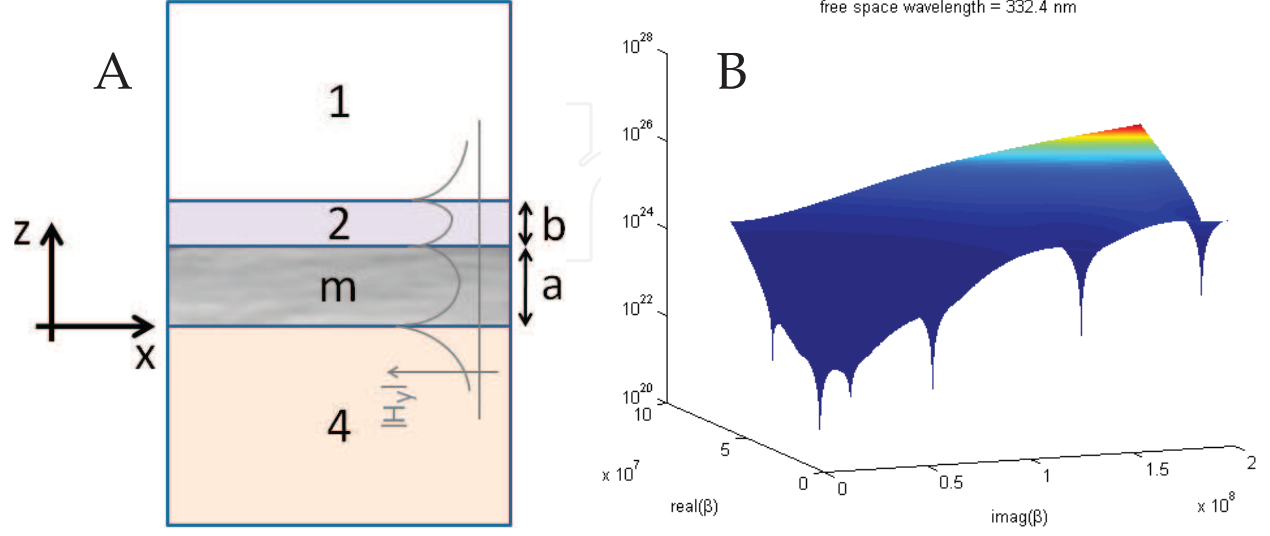
Figure 8. A) Geometry of the IIMI structure. The metal layer is located on the top of a dielectric half-space, and it is covered by a layer of other dielectric with free space above. A sketch of the absolute value of the magnetic field, as expected by modes bound to the interfaces, is also presented. B) Example of absolute values surface of the determinant of the matrix **C** (Equation 63) in the space of complex β for $\lambda = 332.4\,nm$. The minima which converge to zero represent solutions for the dispersion equation of the IIMI structure (Equation 64).

Applying the continuity conditions (Equation 21), we obtain six equations, two for each boundary.

- Boundary 1–2 ($z = a + b$)

$$A_1 e^{-\gamma_1(a+b)} = A_2^- e^{-\gamma_2(a+b)} + A_2^+ e^{\gamma_2(a+b)} \tag{54}$$

$$\frac{\gamma_1}{\varepsilon_1} A_1 e^{-\gamma_1(a+b)} = \frac{\gamma_2}{\varepsilon_2} A_2^- e^{-\gamma_2(a+b)} - \frac{\gamma_2}{\varepsilon_2} A_2^+ e^{\gamma_2(a+b)} \tag{55}$$

- Boundary 2–m ($z = a$)

$$A_2^- e^{-\gamma_2 a} + A_2^+ e^{\gamma_2 a} = A_m^- e^{-\gamma_m a} + A_m^+ e^{\gamma_m a} \tag{56}$$

$$\frac{\gamma_2}{\varepsilon_2} A_2^- e^{-\gamma_2 a} - \frac{\gamma_2}{\varepsilon_2} A_2^+ e^{\gamma_2 a} = \frac{\gamma_m}{\varepsilon_m} A_m^- e^{-\gamma_m a} - \frac{\gamma_m}{\varepsilon_m} A_m^+ e^{\gamma_m a} \tag{57}$$

- Boundary m–4 ($z = 0$)

$$A_m^- + A_m^+ = A_4 \tag{58}$$

$$-\frac{\gamma_m}{\varepsilon_m} A_m^- + \frac{\gamma_m}{\varepsilon_m} A_m^+ = \frac{\gamma_4}{\varepsilon_4} A_4 \tag{59}$$

Substituting $A_1 e^{-\gamma_1(a+b)}$ in Equation 55 by Equation 54 yields

$$\frac{\gamma_1}{\varepsilon_1} \left(A_2^- e^{-\gamma_2(a+b)} + A_2^+ e^{\gamma_2(a+b)} \right) = \frac{\gamma_2}{\varepsilon_2} \left(A_2^- e^{-\gamma_2(a+b)} - A_2^+ e^{\gamma_2(a+b)} \right) \tag{60}$$

Substituting A_4 in 59 by 58,

$$\frac{\gamma_m}{\varepsilon_m}\left(-A_m^- + A_m^+\right) = \frac{\gamma_4}{\varepsilon_4}\left(A_m^- + A_m^+\right) \tag{61}$$

With Equations 60 and 61, we reduced the system to 4 variables: A_2^-, A_2^+, A_m^- and A_m^+. These two equations in addition to Equations 56 and 57 can be written in a matrix form:

$$\mathbf{C}\begin{pmatrix} A_2^- \\ A_2^+ \\ A_m^- \\ A_m^+ \end{pmatrix} = \begin{pmatrix} 0 \\ 0 \\ 0 \\ 0 \end{pmatrix} \tag{62}$$

In which $\mathbf{C}$ is a 4×4 matrix of coefficients:

$$\mathbf{C} = \begin{pmatrix} R_1 e^{-\gamma_2(a+b)} - R_2 e^{-\gamma_2(a+b)} & R_1 e^{\gamma_2(a+b)} + R_2 e^{\gamma_2(a+b)} & 0 & 0 \\ 0 & 0 & R_4 + R_m & R_4 - R_m \\ e^{-\gamma_2 a} & e^{\gamma_2 a} & -e^{-\gamma_m a} & -e^{\gamma_m a} \\ R_2 e^{-\gamma_2 a} & -R_2 e^{\gamma_2 a} & -R_m e^{-\gamma_m a} & R_m e^{\gamma_m a} \end{pmatrix} \tag{63}$$

γ_i and R_i are given by Equations 14 and 42, respectively. For a homogeneous system of linear equations, the non-zero solutions occur when the determinant of the matrix of coefficients is zero:

$$\text{Dispersion relation for IIMI:} \quad |\mathbf{C}| = 0 \tag{64}$$

8.1. Dispersion curves for an IIMI structure

The dispersion curve of this last structure for a Drude's model without damping is presented in Figure 5F. For comparison, the light lines of the dielectrics adjacent to the metal are drawn, as well as the half-spaces of the same dielectrics with the metal. This structure behaves close to an asymmetric IMI. It presents one mode, under the lower half-spaces dispersion. The wavevector of this mode tends to infinity at ω_{sp} of the lower half-spaces dispersion. The mode above the two half-spaces dispersion tends to infinity at ω_{sp} of the other half-spaces dispersion. For lower frequencies, the same mode reaches the low refractive-index light line and it is cut-off (see arrow in Figure 5F).

The dispersion curve and propagation length of the same geometry, but with the silver modelled by the experimental permittivity is drawn in Figure 7E and F. As in the case of the asymmetric IMI structure, the actual one presented three modes. One of the modes that has no PSP character (solution 3). Other mode presents small wavevectors and a cut-off, but longer propagation lengths. Finally, a third mode with great wavevectors and PSP, that bends in the quasi-bound mode, reaching zero. This mode does not appear in the bulk region.

9. Conclusion

We showed, mathematically, the principal properties of propagating surface plasmons. We presented the analysis of plasmons that appear at planar interfaces, such as IM, symmetric and assymetric variants of IMI and MIM, and IIMI. Only for the IM geometry, there is an explicit function $\beta = f(\omega)$ (Equation 28). For the other geometries, the dispersions are

implicit functions[7] (Equations 46, 52 and 64). For these geometries, one can re-arrange the dispersion relations as $f(\beta, \omega) = 0$, and numerically find the zeros for β in the first quadrant, as we can define the propagation towards $+x$, and lossy materials lead to exponential decays of the fields [32].

When modelling the metals as lossless by using the lossless Drude's permittivities, the propagation constants are real. In this case, the wavevectors parallel to the interface diverge at the surface plasmon frequencies. When the metals are modelled as lossy by using complex experimental values of permittivities, the wavevectors do not diverge any more, and the dispersion curves bend forming quasi-bond modes, regions with anomalous dispersion ($d\omega/dk < 0$).

Figure 8B shows an example the surface $|f(\beta, \omega)|$ for the IIMI structure at one specific frequency and using tabulated permittivity of silver. This surface presents many minima. The minima that converge to zero are all solutions of the dispersion relation. Infinite solutions are possible for one single frequency, but the most interesting ones are the solutions with relatively long propagation lengths — from tens of nanometers up. Nevertheless, the solutions with very short propagation lengths are also important for matching the boundary conditions and launching the propagating surface plasmons [32].

Author details

Baltar Henrique T. M. C. M., Drozdowicz-Tomsia Krystyna and Goldys Ewa M.
Faculty of Science of Macquarie University, Department of Physics and Astronomy, Sydney, Australia

10. References

[1] Aroca, R. F., Ross, D. J. & Domingo, C. [2004]. Surface-enhanced infrared spectroscopy, *Applied Spectroscopy* 58(11): 324A–338A.

[2] Bozhevolnyi, S. I. [2009]. *Introduction to surface plasmon-polariton waveguides*, Pan Stanford, chapter 1.

[3] Cheng, D. K. [1989]. *Field and wave electromagnetics*, 2 edn, Addison-Wesley.

[4] Dionne, J. A., Sweatlock, L. A., Atwater, H. A. & Polman, A. [2005]. Planar metal plasmon waveguides: frequency-dependent dispersion, propagation, localization, and loss beyond the free electron model, *Physical Review B* 72(7).

[5] Dionne, J. A., Verhagen, E., Polman, A. & Atwater, H. A. [2008]. Are negative index materials achievable with surface plasmon waveguides? a case study of three plasmonic geometries, *Optics Express* 16(23): 19001–19017.

[6] Fort, E. & Gresillon, S. [2008]. Surface enhanced fluorescence, *Journal of Physics D: Applied Physics* 41(1): 013001.

[7] Homola, J. [2006]. *Electromagnetic theory of surface plasmons*, Springer series on chemical sensors and biosensors, Springer, chapter 1.

[8] Huber, A., Ocelic, N., Kazantsev, D. & Hillenbrand, R. [2005]. Near-field imaging of mid-infrared surface phonon polariton propagation, *Applied Physics Letters* 87(8): 081103.

[9] Hwang, E. H. & Das Sarma, S. [2007]. Dielectric function, screening, and plasmons in two-dimensional graphene, *Physical Review B* 75(20): 205418.

[10] Iskander, M. F. [1992]. *Electromagnetic fields and waves*, Prentice-Hall.

---

[7] Functions not with the strict meaning, as one input may produce many outputs.

[11] Jablan, M., Buljan, H. & Soljačić, M. [2009]. Plasmonics in graphene at infrared frequencies, *Physical Review B* 80(24): 245435.

[12] Jackson, J. D. [1962]. *Classical electrodynamics*, 1 edn, John Wiley and Sons.

[13] Johnson, P. B. & Christy, R. W. [1972]. Optical constants of the noble metals, *Physical Review B* 6(12): 4370–4379.

[14] Junxi, Z., Lide, Z. & Wei, X. [2012]. Surface plasmon polaritons: physics and applications, *Journal of Physics D: Applied Physics* 45(11): 113001.

[15] Kawata, S. [2001]. *Near-field optics and surface plasmon polaritons*, Springer.

[16] Lavoie, B. R., Leung, P. M. & Sander, B. C. [2011]. Metamaterial waveguides, *ArXiv e-prints* .

[17] Le Ru, E. C. & Etchegoin, P. G. [2008]. Surface-enhanced raman scattering (sers) and surface-enhanced fluorescence (sef) in the context of modified spontaneous emission, *ArXiv e-prints* .

[18] Le Ru, E. C. & Etchegoin, P. G. [2009]. *Principles of surface-enhanced Raman spectroscopy and related plasmonic effects*, Elsevier.

[19] Liu, H., Genov, D. A., Wu, D. M., Liu, Y. M., Steele, J. M., Sun, C., Zhu, S. N. & Zhang, X. [2006]. Magnetic plasmon propagation along a chain of connected subwavelength resonators at infrared frequencies, *Physical Review Letters* 97(24): 243902.

[20] Lynch, D. W. & Hunter, W. R. [1985]. *Comments on the optical constants of metals and an introduction to the data for several metals*, Academic Press, Orlando.

[21] Maier, S. A. [2007]. *Plasmonics: fundamentals and applications*, Springer.

[22] Mills, D. L. & Burstein, E. [1974]. Polaritons: the electromagnetic modes of media, *Reports on Progress in Physics* 37(7): 817–926.

[23] Novotny, L. & Hecht, B. [2006]. *Principles of nano-optics*, Cambridge University, Cambridge.

[24] Pendry, J. B., Holden, A. J., Robbins, D. J. & Stewart, W. J. [1999]. Magnetism from conductors and enhanced nonlinear phenomena, *IEEE Transactions on Microwave Theory and Techniques* 47(11): 2075–2084.

[25] Rana, F. [2008]. Graphene terahertz plasmon oscillators, *IEEE Transactions on Nanotechnology* 7(1): 91–99.

[26] Rivas, J. G., Kuttge, M., Bolivar, P. H., Kurz, H. & Sánchez-Gil, J. A. [2004]. Propagation of surface plasmon polaritons on semiconductor gratings, *Physical Review Letters* 93(25): 256804.

[27] Sarid, D. & Challener, W. A. [2010]. *Modern introduction to surface plasmons: theory, mathematica modeling, and applications*, Cambridge.

[28] Sernelius, B. E. [2001]. *Surface modes in physics*, Wiley-VCH.

[29] Staelin, D. H., Morgenthaler, A. W. & Kong, J. A. [1994]. *Electromagnetic waves*, Prentice-Hall.

[30] van Vugt, L. K. [2007]. *Optical properties of semiconducting nanowires*, PhD thesis.

[31] Welford, K. [1991]. Surface plasmon-polaritons and their uses, *Optical and Quantum Electronics* 23(1): 1–27.

[32] Zakharian, A. R., Moloney, J. V. & Mansuripur, M. [2007]. Surface plasmon polaritons on metallic surfaces, *IEEE Transactions on Magnetics* 43(2): 845–850.

[33] Zayats, A. V. & Richards, D. [2008]. *Near-optics and near-field optical microscopy*, Artech House.

[34] Zayats, A. V., Smolyaninov, I. I. & Maradudin, A. A. [2005]. Nano-optics of surface plasmon polaritons, *Physics Reports* 408(3-4): 131–314.